Clim. Past Discuss., 9, 3825–3870, 2013
www.clim-past-discuss.net/9/3825/2013/
doi:10.5194/cpd-9-3825-2013

Climate of the Past Discussions
Open Access

Greenland accumulation and its connection to the large-scale atmospheric circulation in ERA-Interim and paleo-climate simulations

N. Merz[1,2], **C. C. Raible**[1,2], **H. Fischer**[1,2], **V. Varma**[3], **M. Prange**[3], **and T. F. Stocker**[1,2]

[1]Climate and Environmental Physics, University of Bern, Bern, Switzerland
[2]Oeschger Centre for Climate Change Research, University of Bern, Bern, Switzerland
[3]MARUM – Center for Marine Environmental Sciences and Faculty of Geosciences, University of Bremen, Bremen, Germany

Received: 13 June 2013 – Accepted: 25 June 2013 – Published: 9 July 2013

Correspondence to: N. Merz (merz@climate.unibe.ch)

Published by Copernicus Publications on behalf of the European Geosciences Union.

Abstract

Accumulation and aerosol chemistry records from Greenland ice cores offer the potential to reconstruct variability in Northern Hemisphere atmospheric circulation over the last millennia. However, an important prerequisite for a reconstruction is the stable relationship between local accumulation at the ice core site with the respective circulation pattern throughout the reconstruction period. We address this stability issue by using a comprehensive climate model and performing time-slice simulations for the present, the pre-industrial, the early Holocene and the last glacial maximum (LGM). The relationships between accumulation, precipitation and atmospheric circulation are investigated on on various time-scales. The analysis shows that the relationship between local accumulation on the Greenland ice sheet and the large-scale circulation undergoes a significant seasonal cycle. As the weights of the individual seasons change, annual mean accumulation variability is not necessarily related to the same atmospheric circulation patterns during the different climate states. Within a season, local Greenland accumulation variability is indeed linked to a consistent circulation pattern, which is observed for all studied climate periods, even for the LGM, however these circulation patterns are specific for different regions on the Greenland ice sheet. The simulated impact of orbital forcing and changes in the ice-sheet topography on accumulation exhibits strong spatial variability emphasizing that accumulation records from different ice core sites cannot be expected to look alike since they include a distinct local signature. Accumulation changes between different climate periods are dominated by changes in the amount of snowfall and are driven by both thermodynamic and dynamic factors. The thermodynamic impact determines the strength of the hydrological cycle, and warmer temperatures are generally accompanied by an increase in Greenland precipitation. Dynamical drivers of accumulation changes are the large-scale circulation and the local orography having a distinct influence on the local flow characteristic and hence the amount of precipitation deposited in any Greenland region.

CPD
9, 3825–3870, 2013

1 Introduction

Understanding the mass balance of the Greenland Ice Sheet (GrIS) is central to predicting future global sea level changes. Snow accumulation (defined here as snow precipitation minus sublimation) has been identified as the most important variable for the mass balance of the ice sheet (McConnell et al., 2000a,b). Accurate records of accumulation are therefore fundamental to investigate spatial and temporal variations in the mass balance and elevation changes of the polar ice sheets. Greenland ice cores provide high-resolution (annually resolved) ground-based point estimates of accumulation and offer the possibility to retrieve the relationship between climate and accumulation variability (e.g., Banta and McConnell, 2007). Accumulation rates in ice cores are usually calculated by determining annual layers using multiple parameters (e.g., dust, sea-salt, nitrate and $\delta^{18}O$) measured in continuous sample cuts and correcting layer thickness for glaciological thinning (Anklin et al., 1998; Mosley-Thompson et al., 2001). Local ice core accumulation variability is largely attributed to changes in atmospheric circulation rather than to thermodynamic control (Kapsner et al., 1995; Crüger et al., 2004; Hutterli et al., 2007). Based on this, a number of studies identify specific features of the atmospheric circulation, which have an imprint on Greenland accumulation variability: Rogers et al. (2004) showed that increased cyclone activity in the proximity of the accumulation location causes anomalous high accumulation and that cyclone frequency variations are significantly related to the primary modes of Greenland accumulation.

In some studies, the reverse approach is used to reconstruct features of atmospheric circulation from Greenland accumulation variability: Appenzeller et al. (1998b,a) reconstructed the North Atlantic Oscillation (NAO) for several centuries from the NASA-U ice core. However, the agreement among various pre-instrumental NAO reconstructions including NASA-U is not significant (Luterbacher et al., 2001; Pinto and Raible, 2012). A possible explanation for these diverging results is the fact that the centers of action of the NAO are not stationary over time (Raible et al., 2006) resulting in a different imprint

CPD
9, 3825–3870, 2013

on the proxy records (Lehner et al., 2012). To avoid the uncertainties arising from the instabilities in atmospheric modes, Hutterli et al. (2005) have linked inter-annual accumulation variability in different Greenland regions to distinct large-scale atmospheric patterns based on ERA40 reanalysis data. The significant relationship found offers the potential to reconstruct the occurrence of these circulation patterns from ice core derived accumulation records in the according regions. However, an important prerequisite for such reconstructions is the stability of the connection between local accumulation rate at the ice core site and the respective circulation pattern throughout the time of reconstruction. As seen for the NAO reconstruction (Lehner et al., 2012) this requirement is not necessarily fulfilled.

In this study we address this stability issue and use a state-of-art climate model as a testbed to revisit the relationship between local accumulation and these atmospheric circulation patterns, similar to Hutterli et al. (2005). We perform time-slice simulations for the present-day, the pre-industrial, the early Holocene and the last glacial maximum (LGM) to cover a variety of past climate states. Besides the stability issue, which is of great value for the proxy interpretation, we use the model to investigate the influence of orbital forcing and moderate changes in the Greenland ice sheet topography on the GrIS mean accumulation. The sensitivity to topographic changes is studied with a set of simulations which implement reconstructed ice sheet topographies from Peltier (2004) for the early Holocene. Moreover, we study in detail the relationship of local GrIS accumulation and atmospheric circulation variability as we observe distinct seasonal features, which have not been depicted in the studies using annual mean accumulation.

The manuscript is structured as follows: Sect. 2 describes the observational data, the model and the experiments and includes a short description of the statistical analysis tools. In Sect. 3 we present the model results regarding Greenland accumulation during different climate states and investigate the influence of the external forcing on total and local GrIS accumulation. Section 4 is focusing on the relationship between local GrIS accumulation/precipitation and the prevailing atmospheric circulation patterns on various time-scales (daily to annually). Moreover, tests on the stability of the deducted

CPD
9, 3825–3870, 2013

atmospheric circulation patterns in the different time-slice simulations are presented. All results are discussed in Sect. 5 and the conclusions are presented in Sect. 6.

2 Data and method

2.1 Reanalysis data

The atmospheric reanalysis dataset used in this study is the ERA-Interim (ERAi) product from the European Centre for Medium-Range Weather Forecasts (ECMWF) (Dee et al., 2011). ERAi data is originally calculated with T255 (~ 80 km) resolution and available on the regular $1^\circ \times 1^\circ$ grid. We use both monthly and daily mean data for the period of 1979–2011. Note that the daily mean surface flux fields, i.e., snowfall, total precipitation, sublimation (also referred to as snow evaporation), are calculated as the 0 to 36 h accumulation forecast minus the 0 to 12 h accumulation forecast to avoid known spin-up effects (Uppala et al., 2005; Dee et al., 2011). In addition to ERAi, all analyses were carried out with ERA40 data (1958–2001). However, the ERA40 results were very similar to ERAi thus only ERAi results are presented here.

2.2 Climate model

Besides the reanalysis data, the study is based on simulations with the Community Climate System Model (version 4, CCSM4) developed at the National Center for Atmospheric Research (NCAR) in a horizontal resolution of $0.9^\circ \times 1.25^\circ$ (Gent et al., 2011). The model includes components for atmosphere, ocean, land and sea ice that communicate through a coupler. We run the CCSM4 with the atmosphere-land-only setup which consists of the Community Atmosphere Model version 4 (Neale et al., 2010) with a finite volume dynamical core and the Community Land Model version 4 (Oleson et al., 2010) excluding the integrated carbon-nitrogen cycle. Since the setup asks for prescribed lower boundary conditions the model's ocean component is replaced by

CPD
9, 3825–3870, 2013

a data input model. The sea ice model, the Community Ice CodE version 4 (Hunke and Lipscomb, 2008), is used in its thermodynamic-only mode.

2.3 Experiments

To study the accumulation and the associated atmospheric circulation on Greenland during different recent climate states, a set of time-slice experiments is conducted covering four different time periods:

- A present-day (PD) simulation with perpetual 1990 AD condition which is mainly used for model evaluation by comparing with reanalysis data.
- A pre-industrial (PI) simulation with perpetual 1850 AD conditions used as reference simulation for the paleo simulations since it describes the present climate without perturbation by human activities.
- Four early Holocene (EH) simulations with perpetual 8 ka (8000 yr before 1950) conditions but different ice-sheet forcings (see Fig. 1 and Sect. 2.4 for more details).
- A last glacial maximum (LGM) simulation with full glacial conditions including major ice sheets (see Fig. 1). This simulation has previously been used and described by Hofer et al. (2012a,b).

The set of EH simulations is used to test the sensitivity of an interglacial climate to moderate changes in the ice-sheet distribution. These sensitivity experiments are also the reason why the Holocene experiments are placed within the early Holocene (8 ka) instead of the classical Mid-Holocene (6 ka) setup as used in the Paleoclimate Modeling Intercomparison Project (PMIP) protocol (Braconnot et al., 2007). During the early Holocene sea-level estimates show a considerable sea-level rise resulting from significant changes in the size of the ice-sheets (see e.g., Smith et al., 2011 and references therein). However, between 7 ka and present sea-level changes have been comparably small so the mid-Holocene ice sheets are similar to the present state. A list of all

CPD
9, 3825–3870, 2013

simulations and the external forcing factors used is provided in Table 1. All simulations are conducted for 33 model years and the analysis is based on the last 30 yr of each simulation as the first 3 yr are declared as spin-up phase.

2.4 Boundary conditions

The sea-surface temperature (SST) and sea ice fields used as lower boundary conditions in the model experiments are taken from appropriate outputs of fully-coupled CCSM3 simulations. These are conducted with the low-resolution CCSM3 (Yeager et al., 2006) model version. For our PD simulation we use output of a CCSM3 control 1990 AD run (provided by Earth System Grid). For the PI simulation we use output of a control 1850 AD simulation (Merkel et al., 2010) and for the EH simulations we take 33 yr output of around 8 ka from a transient Holocene simulation. This transient Holocene simulation starts at 9 ka and is similar to the CCSM3 run by Varma et al. (2012) except that no orbital acceleration is applied. For all time-slice simulations, the monthly mean SST and sea ice output of the corresponding CCSM3 simulations are used as time-varying lower boundary conditions. With this setup we account for both, the different states of the ocean and sea ice cover during the different climate periods as well as for inter-annual variability in the SSTs and sea ice concentration.

The values for the Earth's orbital parameters are calculated according to Berger (1978). The influence of the orbital forcing difference between present-day and pre-industrial is negligible. Similar as for the mid-Holocene (e.g., Braconnot et al., 2007), for 8 ka the orbital parameters lead to an enhanced seasonal cycle of the incoming solar radiation (insolation) in the Northern Hemisphere (NH). The largest signal is a distinct increase (up to 40 $W m^{-2}$) for the NH high latitude summer insolation. The larger tilt of the earth axis also results in an increase in annual mean insolation in the high latitudes of both hemispheres. For the LGM, the orbital forcing difference compared with pre-industrial is more moderate with the largest signal being a decrease in summer insolation (up to 14 $W m^{-2}$) in the high-latitudes of both hemispheres.

CPD
9, 3825–3870, 2013

The greenhouse gas (GHG) concentrations are set according to the PMIP protocol. As an exception, for the EH simulations we use pre-industrial GHGs to be consistent with the respective CCSM3 Holocene simulation (Varma et al., 2012), which provides the SST and sea ice fields for these experiments. This means that the EH simulations aside from the different ice sheets are solely driven by orbital forcing with respect to PI.

The set of four EH simulations differ in the implemented topography and size of the global ice sheets: whereas EH_{PD} includes the present-day mask as PD and PI do, for $EH_{7\,ka}$ the reconstruction for 7 ka by the ICE-5G model by Peltier (2004) is implemented. Equivalent to $EH_{7\,ka}$ we used the ICE-5G reconstructions for 8 and 9 ka for the $EH_{8\,ka}$ and the $EH_{9\,ka}$ simulation, respectively. To investigate the sensitivity of the paleo topographies and ice sheets we declare EH_{PD} as the reference simulation for the early Holocene against which we compare the other EH simulations.

The topography changes in the NH with respect to the present-day mask can be summarized as follows: the 7 ka (Fig. 1a) topography shows some slightly lower areas in North America and Scandinavia since the post-glacial rebound effect following the melting of the Laurentide and the Fennoscandian ice domes has not been completed at that time. At the same time, North Greenland is slightly higher and up to 500 m lower at the central eastern and south western coast, respectively. For 8 ka (Fig. 1b), the differences to the present mask are similar as for 7 ka but stronger. The 9 ka mask (Fig. 1c) is marked by significant remnants of the Laurentide ice sheet around the Hudson Bay. In addition, 9 ka Greenland is higher than present particularly in coastal areas. The LGM simulation contains full glacial conditions with large Laurentide and Fennoscandian ice sheets (see Fig. 1d). To account for the presence of the large ice sheets, the sea level in the LGM simulation is lowered by 120 m with respect to modern levels. In contrast, the sea level changes corresponding to the included early Holocene ice sheets are not implemented in the EH simulations since they are rather small (< 20 m).

CPD
9, 3825–3870, 2013

2.5 Correlation and composite analysis

We apply classical correlation and composite analyses to derive the relationship between GrIS accumulation variability and the state of the large-scale circulation. Similar to Hutterli et al. (2005) we primarily look at accumulation in four different Greenland regions (see Fig. 2): central-western (CW; 70–75° N, 40–50° W), north-eastern (NE; 76–82° N, 30–40° W), south-west (SW; 63–66° N, 47–48° W) and south-east (SE; 63–65° N, 44° W, 64–66° N, 43° W, 65–66° N, 42° W). The accumulation rates in these four regions are representative for larger areas of the GrIS (shaded areas in Fig. 2). For each region a series of standardized and detrended pseudo accumulation records are generated. Following that, the accumulation records are correlated with the 500 hPa geopotential height (z500) field to come up with specific correlation patterns for each accumulation region. In addition, we calculate two kinds of z500 composite patterns: the plus-minus composite pattern is defined as the subtraction of the mean of all cases when accumulation is ≤ -1 standard deviation from the mean of all cases when accumulation is ≥ 1 standard deviation. Hence, the plus-minus composite pattern accounts for the accumulation magnitude between a high and a low accumulation year. We apply the plus-minus composites to annual mean accumulation (which is applicable for ice core data) as well as to seasonal mean accumulation to identify possible seasonal dependencies. Further positive composite patterns are deduced, i.e. the mean z500 pattern of all cases when accumulation is ≥ 1 standard deviation (expressed as anomaly from the z500 climatological mean pattern). These positive composite patterns are applied to daily snowfall/precipitation time series to study the daily weather situations leading to a local precipitation/snow event in the different Greenland regions and during the different seasons. To compensate for sub-seasonal biases within these daily accumulation time series, the annual cycle is removed beforehand. Note also that a fixed present-day calendar was used to define the seasonal mean values of all simulations.

CPD
9, 3825–3870, 2013

3 Greenland accumulation in different climate states

3.1 Present-day accumulation

Present estimates of the GrIS accumulation are based on accumulation records from ice cores and snow pits as well as on atmospheric data from reanalysis and coastal weather stations (Bales et al., 2009). Mean accumulation rates are estimated to be around 300 mm yr^{-1} (see Hakuba et al., 2012 and references therein). The representation of GrIS accumulation in reanalysis datasets has been evaluated by Chen et al. (2011). They show that regarding both, spatial distribution and temporal variability ERAi resembles best the observations compared to other reanalyses. Accumulation generally increases from northern to southern Greenland and is highest in southern coastal areas (Fig. 3a), where we also find the strongest cyclonic activity (Dethloff et al., 2002). The CCSM4 simulation with present-day climate (PD) is able to realistically represent spatial accumulation variability (Fig. 3b). However, accumulation is overestimated in most areas. This overestimation is mainly attributed to a positive model bias in Greenland precipitation and to a cold summer bias leading to an overestimation of summer snowfall at the expense of rain in South Greenland. The resulting mean accumulation rates for the entire GrIS are 306 mm yr^{-1} for ERAi and 346 mm yr^{-1} for PD demonstrating that ERAi is very close to the observed estimates whereas the model clearly overestimates ($\sim$ 15 %) accumulation on average. Nevertheless, the spatial distribution of accumulation (both mean and variability) in the PD model simulation mainly resembles the observed distribution. Thus, we are sufficiently confident to use the CCSM4 model for studying GrIS accumulation during past climate states.

3.2 Accumulation during the early Holocene and the LGM

To gain a first impression of Greenland accumulation during past climate conditions, we compare the EH_{PD} and the LGM simulations against PI, i.e. the reference for the paleo simulations. The climate in EH_{PD} is comparable to the one in the PMIP2 mid-Holocene

CPD
9, 3825–3870, 2013

simulations (Braconnot et al., 2007) as the orbital forcing is the dominant factor. The NH EH_{PD} climate has an enhanced seasonal cycle, i.e. warmer summers and colder winters particularly over continental areas compared with PI. In the Arctic ocean, however, the summer warming leads to a warming of the Northern high latitudes all year round due to feedback mechanisms, e.g., albedo-induced warming due to decreased NH sea-ice in all seasons, similar to the findings by Fischer and Jungclaus (2011). The changes in the hydrological cycle in Greenland are more diverse: during winter, snowfall increases along the Greenland East coast due to the increased moisture availability and moderate atmospheric circulation changes, which lead to stronger flow to Greenland from the East (not shown). In summer, the EH_{PD} exhibits a distinct increase in precipitation in most of Greenland coming along with the summer warming. However, precipitation which occurs along coastal regions and particularly in South Greenland falls mostly in form of rain due to the warmer temperatures. Hence most of the precipitation increase is not relevant for snow accumulation. The resulting annual mean snowfall (Fig. 4a) increases over inland Greenland along the main ridge and at the East coast. Along the rest of the coastal areas we find rather a decrease in snowfall at the expense of rain. The increased temperatures also lead to stronger sublimation in these lower areas along the coast (not shown) contributing to the accumulation pattern in Fig. 4c with lower accumulation in coastal areas except for the Southeast. There, as well as for most of central Greenland, the increased snowfall leads to higher accumulation in EH_{PD} than for PI. The GrIS mean values (Table 2) show that the spatially diverse accumulation changes almost compensate each other so the GrIS mean accumulation rate for EH_{PD} stays with $300\,mm\,yr^{-1}$ at the PI level.

As described in Sect. 2.4 the orbital parameters during the LGM are not as different from the present-day setup. The dominant boundary conditions for the LGM are the low GHG concentrations and the extensive ice sheets which are the result of the fact that the LGM is preceded by a glacial period of almost 100 000 yr. The LGM forcing leads to a broad cooling (compared to PI conditions), which is mostly expressed in the NH mid- and high latitudes. The cooling causes large-scale reduction of moisture in the NH

CPD
9, 3825–3870, 2013

polar region resulting in a distinct slow-down of the hydrological cycle. Snowfall over GrIS is reduced in all regions (see Fig. 4b) with the strongest reduction along the main accumulation regions. The fact that due to the colder climate the sublimation rates are reduced as well (not shown), can by no means compensate the precipitation reduction. Thus the LGM-PI accumulation change (Fig. 4d) is clearly dominated by the change in snowfall. In addition, the dry Greenland conditions are explained by the fact that with the presence of the extensive Laurentide ice sheet the Atlantic storm track is shifted southwards (Hofer et al., 2012a,b). Therefore, North Atlantic areas which presently experience a lot of precipitation (South Greenland, British Isles, Scandinavia), have a much drier climate during LGM. The GrIS mean values of the hydrological cycle (Table 2) show a drop to approximately 30 % of the PI levels in all quantities proving that the interglacial-glacial difference in Greenland accumulation is remarkable.

3.3 Sensitivity to moderate changes in GrIS topography

To quantify the effect of the different Holocene ice sheet masks on GrIS accumulation we compare the EH simulations with paleo topographies ($EH_{7\,ka}$, $EH_{8\,ka}$ and $EH_{9\,ka}$) against EH_{PD} to identify the pure ice sheet sensitivity with all other boundaries conditions held constant. Thereby, we observe in all experiments a remarkable influence of the ice sheet topography on GrIS snowfall (Fig. 5a, b, c). Dominated by these changes in snowfall, accumulation changes equivalently in all three EH simulations with paleo topographies (Fig. 5d, e, f).

In $EH_{7\,ka}$ and $EH_{8\,ka}$ the Greenland ice sheet is narrowed in the south-western and the central-eastern part whereas the rest of Greenland is several hundred meters higher than present (see Fig. 1a, b). The lowered regions experience a local warming at the surface (Fig. 6a, b), which results in a local increase of annual sublimation but does not significantly affect the accumulation anomalies. The lowering of the south-western and the central-eastern flanks of GrIS displaces the steep slopes inland shifting the main precipitation (snowfall) regions in a similar way. The analysis of the vertical motion over the GrIS for $EH_{7\,ka}$-EH_{PD} and $EH_{8\,ka}$-EH_{PD} (Fig. 6d, e) confirms this process:

CPD
9, 3825–3870, 2013

enhanced vertical velocities (expressed as wind divergence reduction at 850 hPa and wind divergence increase at 500 hPa) are found on the inland side, whereas close to the south-western and central-eastern coast the flattening causes downward motion anomalies. The lifting of the air masses then leads to an increase in local snowfall and vice-versa for local downward flow anomalies (compare Figs. 5a, b and 6a, b). The distinct decrease in snowfall (and accumulation) in $EH_{7\,ka}$'s and $EH_{8\,ka}$'s south-western Greenland is additionally strengthened by a moderate change in the atmospheric circulation. Thereby both, $EH_{7\,ka}$ and $EH_{8\,ka}$, exhibit a change in the annual mean circulation, which result in an enhanced flow from the East to Greenland (not shown). Similar as for EH_{PD}-PI (Fig. 4a) this anomalous westward flow leads to increased snowfall over the steep slopes of East Greenland (particularly in $EH_{7\,ka}$, Fig. 5a) whereas on the lee side (West Greenland) snowfall is decreased. Regarding the GrIS mean accumulation rates (Table 2), the 8 ka ice sheet setup leads to a reduction of GrIS mean snowfall and accumulation whereas $EH_{7\,ka}$ roughly remains on the EH_{PD} level.

In the $EH_{9\,ka}$ simulation the Greenland ice sheet is about 500 m higher (Fig. 1c), particularly in coastal regions making the flanks of the ice sheet even steeper. Over the main ice sheet body the increased orography results in a widespread cooling of a few degrees Celsius (Fig. 6c). The snowfall and accumulation sensitivity of the topographic changes, however, also seem to be rather controlled by the atmospheric flow characteristics. The steepening of the ice sheet flanks results in anomalous upward flow (Fig. 6f) and increased snowfall in coastal regions especially in western and southern Greenland (Fig. 5c). At the same time, in the adjacent inland areas of the coast the wind divergence indicates downward motion anomalies resulting in less snowfall in these regions. The resulting GrIS mean accumulation (Table 2) of $EH_{9\,ka}$ is slightly decreased compared with EH_{PD} since the snowfall reduction over inland Greenland outweighs the increase in the coastal areas.

CPD
9, 3825–3870, 2013

4 Accumulation variability and its relationship to atmospheric circulation

4.1 Annual mean relationship

Besides changes due to various climate forcings in the mean accumulation, local accumulation shows remarkable inter-annual variability. As described in Sect. 2.5, we generate pseudo accumulation records for four Greenland regions (Fig. 2) and calculate the correlation and plus-minus composite patterns to find links between local accumulation and atmospheric circulation variability. Hutterli et al. (2005) applied this method to ERA40 annual mean data and found distinct large-scale atmospheric circulation patterns for three of four of these pseudo accumulation records. For ERAi we find very similar patterns for these three regions (Fig. 7a): accumulation variability in the CW region is related to an inverted NAO-pattern: positive accumulation anomalies are associated with a high-pressure blocking south of Greenland equivalent to a negative NAO-like pattern and vice-versa for negative accumulation anomalies. The blocking of South Greenland leads to an enhanced flow to central-western Greenland and thus results in stronger local snowfall and eventually in increased accumulation. The circulation pattern associated with SW accumulation shows anomalous strong westerly flow to South Greenland due to a low pressure system over North Greenland and a high pressure situation over the North Atlantic westwards of the British Isles. For high SE accumulation another blocking-like pattern is found with a high pressure centered over the Norwegian Sea. The SE pattern further shows two low pressure anomalies over the Labrador Sea and western Russia. The resulting circulation transports moist air masses to south-eastern Greenland. Note that all three (CW, SW and SE) patterns have also an imprint on the European climate due to their large-scale nature (see Hutterli et al. (2005) for more details). For accumulation in the NE region we find a weak pattern (not shown) resembling Hutterli et al. (2005). They relate NE accumulation variability rather to the local cyclone frequency than to a distinct large-scale circulation pattern.

CPD
9, 3825–3870, 2013

To test the stability of these patterns for earlier climate states, we apply the correlation and composite analysis to all model simulations. First, the model is evaluated by comparing the PD patterns (Fig. 7d, e, f) against ERAi (Fig. 7a, b, c). In order to add quantitative estimates of the consistency of these patterns we calculate the pattern correlation of the z500 plus-minus composites for the North Atlantic domain (indicated by the black frame in Fig. 7a). The significance level for the pattern correlation is determined by applying auto-correlation analysis on the z500 data in the North Atlantic domain. The resulting estimate for the number of spatially independent grid points within this domain points out that pattern correlation values $r \geq 0.50$ are significant at the 5 %-level according to t test statistics. The model exhibits variable ability in reproducing the atmospheric patterns of ERAi: the negative NAO-like pattern for CW accumulation is only coarsely represented in PD with an insignificant high-pressure anomaly shifted eastwards compared with ERAi. The CW accumulation of the model seems rather to be linked to a low pressure system over North Greenland. The visual differences between the ERAi and PD CW-patterns are evident by a very low pattern correlation ($r_{\text{ERAi-PD}} = -0.18$). In contrast, for SW accumulation the model resembles the main pressure anomalies found in ERAi which is reflected in a high pattern correlation of $r_{\text{ERAi-PD}} = 0.76$. Hence, the model indeed captures the relationship between local SW accumulation and the large-scale circulation found in the reanalysis. Regarding the SE-pattern, the PD simulation represents to some extent the blocking over the Norwegian Sea and the low pressure anomalies over the Labrador Sea and Russia found in ERAi. However the pattern correlation shows little agreement ($r_{\text{ERAi-PD}} = 0.33$) owing to the fact that the model simulates a distinct low pressure anomaly over Central Europe for high SE accumulation, a signal which cannot be found in reanalysis data.

Due to the limited ability of the model in simulating the connection of local accumulation and atmospheric circulation, the preconditions for testing the stability of these patterns in the paleo simulations within the model framework are not sufficiently reached (except for SW). To identify the origin of this model bias we extend the analysis to the seasonal and even daily time-scale in order to check whether the model exhibits

CPD
9, 3825–3870, 2013

an improved capability of reproducing the link between Greenland accumulation and atmospheric circulation on shorter time-scales.

4.2 Seasonal mean relationship

Calculating the z500 correlation and plus-minus composite patterns with seasonal mean accumulation data, the relationship between accumulation variability and the circulation patterns shows a remarkable seasonal cycle in both, ERAi and the model (Fig. 8). The winter (DJF) mean accumulation in the three regions is connected with similar patterns as the ERAi annual mean accumulation (compare Figs. 7a and 8a, b). As an exception the SE winter pattern differs from the annual pattern in the position of the western low-pressure anomaly, which is located south of Greenland in summer but over the Labrador Sea in the annual mean. However, the rest of the winter patterns and their annual equivalents show a high similarity suggesting that winter variability is strongly recorded in the annual mean signal. All three winter patterns show a large-scale structure spanning the North Atlantic and at least partly the Europe domain. The summer (JJA) circulation patterns (Fig. 8c, d) exhibit much weaker pressure patterns, which is expected since the pressure variability in the warmer summer season is generally reduced compared to the winter season. Moreover, the summer patterns show little large-scale characteristics and are rather centered over Greenland. The summer CW pattern shows a weak cyclonic anomaly over North Greenland and a weak antipole South of Greenland resulting in westerly flow to Central Greenland. The SW pattern is somewhat similar but shifted to the South so that the snow falls over south-western instead of central-western Greenland. Summer accumulation in the SE is associated with a wave-like pattern with high-pressure anomalies over the Great Lakes and East of Greenland and a low-pressure anomaly in between centered over the Labrador Sea. In contrast to the annual mean patterns (Fig. 7), the PD model simulation reproduces the ERAi patterns fairly well on the seasonal mean scale in both the winter (compare Fig. 8a and b) and the summer (compare Fig. 8c and d) season. The pattern correlation between the ERAi and PD winter plus-minus composites confirms this agree-

CPD
9, 3825–3870, 2013

ment exhibiting the strongest conformance for CW ($r_{\text{ERAi-PD}} = 0.88$), followed by SW ($r_{\text{ERAi-PD}} = 0.64$) and SE ($r_{\text{ERAi-PD}} = 0.52$). For the summer plus-minus composites the pattern correlation shows fairly high values for all three regions (CW: $r_{\text{ERAi-PD}} = 0.60$, SW: $r_{\text{ERAi-PD}} = 0.64$, SE: $r_{\text{ERAi-PD}} = 0.52$).

The seasonal mean analysis is also conducted for spring (MAM) and autumn (SON). The resulting patterns (not shown) associated with regional accumulation variability are somewhat a transition between the summer and winter patterns. This is observed for both, ERAi and PD. Further, when applying the correlation and plus-minus composites to seasonal mean precipitation instead of accumulation data, the resulting patterns (not shown) are equivalent to the seasonal patterns (Fig. 8) diagnosed from accumulation.

In the next step we address the question why the model's ability in reproducing the ERAi annual patterns is limited (see Sect. 4.1) but at the same time the model's seasonal circulation patterns conform well with ERAi. The reason for this model-reanalysis disagreement is investigated by the analysis of the seasonal contributions to the annual signal. For all three regions, we find in ERAi and PD a substantial contribution of every season to the annual mean accumulation, e.g., for CW accumulation in ERAi each of the four seasons delivers at least 20 % of the total yearly accumulation. Therefore the annual mean signal is interpreted as a mixture of all seasons and is (at least in present climate) not solely dominated by one season.

The same relationship between annual and seasonal signals is found for accumulation variability in the three regions (Fig. 9). In particular in the CW and SW region, we find for ERAi almost equal contributions of all seasons to the annual variability signal. In the SE annual variability signal the winter clearly outweighs the summer signal but the contributions of spring an autumn remain substantial. Comparing ERAi and PD it becomes apparent that the seasonal contributions in the model clearly differ from ERAi, at least for CW (Fig. 9a) and SE (Fig. 9c). In both regions the model overestimates summer variability at the expense of the winter variability. This difference is likely connected to the positive model bias in summer snowfall, which is caused by too cold GrIS summer temperatures. The seasonal variability distribution for the SW region (Fig. 9b)

CPD
9, 3825–3870, 2013

in the PD simulation closely matches ERAi. Hence, the annual variability signal of both are comparable since they contain the same weighting of the seasons. Therefore it is no surprise that the annual mean SW pattern (Fig. 7) shows good agreement between PD and ERAi whereas the CW and SE patterns in PD hardly match the ERAi equivalents. When using the ERAi seasonal contributions to the annual accumulation variability from Fig. 9 as weights to add the seasonal patterns to so-called "corrected annual patterns", we come up with a good agreement of PD and ERAi as indicated by significant pattern correlations for all three regions ($r_{\text{ERAi-PD}}$ = 0.75, 0.93 and 0.88). This confirms that the model's problem in correctly representing the CW and SE annual plus-minus composites (Fig. 7) is mainly a problem of weighting the seasonal contributions rather than the representation of the large-scale circulation pattern connected with local GrIS accumulation.

4.3 Recorded circulation patterns in precipitation events

To ascertain the influence of atmospheric circulation on local Greenland accumulation we extend our investigations to the daily (weather) time-scale. For this purpose we identify the z500 circulation patterns associated with a local precipitation event, defined as a day on which precipitation is ≥ 1 standard deviation. Thereby the resulting circulation patterns in ERAi are the same regardless if the analysis is applied to total precipitation or solely snowfall events (for the model this comparison is not possible due to lack of daily snowfall output). For both ERAi and the PD simulation we find similar circulation patterns linked with such precipitation events. As the seasonal mean patterns, the daily patterns show distinct differences between the winter and summer season (compare Fig. 10a, b with Fig. 10c, d). In general, the patterns associated with a local precipitation event are similar to the circulation patterns related to the seasonal mean accumulation variability (compare Fig. 10 with Fig. 8) in the corresponding regions. Winter precipitation in CW is connected with a negative NAO-like situation where Southern Greenland is blocked by a strong anti-cyclone, whereas moist air from the southwest reaches the central and northern part of Greenland's west coast. Winter

CPD
9, 3825–3870, 2013

precipitation events in the SW regions are similarly caused as the ones in the CW region but with a negative NAO-like pattern shifted to the south, so South Greenland is not blocked anymore and the westerlies can bring moist air to SW. Daily precipitation events in SE during winter are linked with the so-called Scandinavian blocking pattern (Yiou et al., 2012) with a cyclonic system Southwest of Greenland and a blocking over the Norwegian Sea. The resulting circulation transports relatively warm and moist air to SE Greenland. For the summer season (Fig. 10c, d), we find again weaker pressure patterns, which resemble the patterns found in the seasonal mean analysis. All summer patterns are spatially limited to Greenland's vicinity and hardly include any signal in the North Atlantic domain. CW and SW precipitation results from westerly wind conditions caused by a low pressure anomaly on the North and a high pressure anomaly on the South side of the precipitation region. Precipitation in the SE region is associated with the same wave-like pattern found for summer mean accumulation (Fig. 8c, d). Thereby moist air is advected from the South to the steep slopes in SE Greenland where it rains out.

All daily circulation patterns of the PD simulation (Fig. 10b, d) highly agree with the ERAi equivalents (Fig. 10a, c). The pattern correlation of the z500 positive composites for the North Atlantic domain shows very high values for all six patterns ($0.81 \leq r_{\text{ERAi-PD}} \leq 0.98$). The remarkable degree of consistency is explained by the fact that the daily patterns are based on an extensive sample (over 2700 daily values) compared to just 30 seasonal or annual mean values used in Sects. 4.1 and 4.2.

4.4 Stability during past climate states

In the previous sections we showed that local GrIS precipitation and accumulation variability on various time-scales is significantly linked to specific circulation patterns. Further, the climate model is to some extent capable of reproducing the patterns found in the ERAi reanalysis. However, to take up the idea of reconstructing atmospheric circulation variability from Greenland accumulation data or precipitation proxies we further assess the stability of these relationships. In doing so, the PD composites for the

CPD
9, 3825–3870, 2013

annual, seasonal and daily accumulation/precipitation indices are compared with the patterns of the paleo climate simulations (Table 3). The stability is again quantified by the pattern correlation for the North Atlantic domain as in Sects. 4.1–4.3.

The highest agreement among the patterns from the different simulations is found for daily precipitation (see Fig. 10c, d for PD patterns). During both the winter and summer season the precipitation events in the PI and all EH simulations show the same positive composite patterns as PD which is confirmed by pattern correlation values ≥ 0.90 (see Table 3). Daily LGM patterns are also in agreement with PD ($0.65 \leq r_{\text{PD-LGM}} \leq 0.94$). This means that although the NH atmospheric circulation during the LGM strongly differs from the present-day conditions (Hofer et al., 2012b), the relative daily weather patterns (anomalies from the seasonal means), which lead to precipitation over any of the three Greenland regions largely remain the same.

The seasonal mean relationship between accumulation variability and the corresponding circulation patterns exhibits reasonable stability throughout the paleo simulations (see Table 3). In particular, the winter patterns generally show strong consistency with most patterns correlation values ≥ 0.70. However, there are also a few exceptions: CW: $r_{\text{PD-EH}_{8\,\text{ka}}} = 0.18$, SW: $r_{\text{PD-EH}_{8\,\text{ka}}} = 0.27$ and SE: $r_{\text{PD-LGM}} = 0.20$. The latter is likely caused by the fact that during LGM winters snowfall is strongly reduced and as a consequence accumulation variability almost vanishes. This leads to a small number of cases captured in the plus-minus composite, so the LGM winter patterns should be treated with caution. Concerning the $\text{EH}_{8\,\text{ka}}$ SW and CW winter patterns the low pattern correlation is caused by a deviating signal in far-field areas (e.g., North America and Europe). The $\text{EH}_{8\,\text{ka}}$ patterns indeed compare well to the PD patterns over Greenland and the North Atlantic domain, so no fundamental change in the relationship of winter accumulation and atmospheric circulation is observed.

The summer plus-minus composite patterns demonstrate quite good consistency in all model simulations with an average pattern correlation ≥ 0.60. Exceptions are the $\text{EH}_{8\,\text{ka}}$ SW and LGM SE patterns. In the $\text{EH}_{8\,\text{ka}}$ simulation the orography of the 8 ka mask lead to an almost complete lack of snowfall and accumulation (partly at the

CPD
9, 3825–3870, 2013

expense rain) in SW Greenland during the summer season. This signal is also reflected in the annual mean $EH_{8\,ka}$-EH_{PD} anomaly (Fig. 5b, e). Thus, the SW accumulation variability signal and the related z500-composites are not very trustworthy. Comparing the SW plus-minus composites based on precipitation of PD and $EH_{8\,ka}$ (not shown) the pattern correlation is 0.89 showing that there is no fundamental change in the connection of SW precipitation and the circulation pattern for $EH_{8\,ka}$ summers as also indicated by the stability of the daily patterns.

For the annual mean accumulation patterns we find limited stability throughout the model simulations (see Table 3, upper left part). In particular, the annual mean CW z500 plus-minus composite shows almost no consistency with pattern correlation values below 0.3 for all comparisons. However, as discussed in Sects. 4.1 and 4.2 the CW patterns in the PD simulation clearly differ from the ERAi pattern due to the overestimation of the summer accumulation variability (see Fig. 9). Accordingly, the model's CW annual patterns should be treated with caution. Regarding the SW annual patterns we observe medium stability throughout the model simulations. Thereby we identify good agreement around Greenland but less agreement over Europe and other more distant regions. The highest pattern correlations are found for the SE region making accumulation in this area the only annual mean signal found to be consistently linked with the same large-scale atmospheric pattern in all simulated climate states. For the CW and SW regions, however, a stable relationship between the annual accumulation variability signal and the associated circulation pattern is not confirmed by the model results.

As already presented in Sect. 4.2, seasonality within the relationship of local GrIS accumulation and the atmospheric circulation is a major issue. Since the annual mean accumulation signal adds up substantial portions of all four seasonal variability signals, a change in the contribution of each season to the annual signal is a critical quantity. As a consequence, even if the accumulation-atmospheric circulation links remain stable throughout the different climate states during each season, differences in the relationship of the seasonal to the annual signal can cause the latter to be unstable

CPD
9, 3825–3870, 2013

as discussed in Sect. 4.2. Assessing the seasonality in the model simulations shows that the seasonal contributions to the annual variability signal vary among the different climate states (Fig. 9). Thereby the seasonal contributions exhibit sensitivity to the various forcings, so either changes in the orbital parameters or changes in the Greenland orography can have an impact on the inter-seasonal distribution of accumulation variability. In most cases the seasonal variability contribution to the annual accumulation signal goes along with the change in the mean accumulation, e.g., with a relative increase of summer accumulation at the expense of winter mean accumulation we observe an equivalent shift in the variability signal. During the early Holocene the orbital forcing leads to an increase in the CW summer accumulation whereas the accumulation in the other seasons is rather decreased. This results in a larger contribution of summer variability in the annual accumulation signal (Fig. 9a). The SE winter accumulation during the LGM almost completely vanishes due to the glacial shift in the storm track so the winter accumulation variability signal contribution to the annual signal is highly decreased (see Fig. 9c).

5 Discussion

As seen in Sect. 3 GrIS accumulation is strongly influenced by various forcing factors. Furthermore, the differences in accumulation between different climate states exhibit strong spatial variability emphasizing that accumulation records from different ice core sites likely differ due to the distinct local characteristics. This independence between different regions is also valid regarding inter-annual accumulation variability as also previously shown by Hutterli et al. (2005), whose regional accumulation indices are not significantly correlated with each other (with the exception of CW and SW). Therefore, an accumulation record derived from a Greenland ice core is just representative for the local Greenland region but not for the entire ice sheet.

To discuss the variety of climate signals included in such an accumulation record, we calculate the pseudo accumulation record for three of the four Greenland regions

CPD
9, 3825–3870, 2013

(Fig. 11) using the model simulations. Note that due to the time-slice setup, the records are not continuous. Still they show the impact of different forcing factors on the local accumulation signal. Due to the spatial independence the three pseudo records only coincide with respect to some forcings (e.g., recent GHG increase or glacial conditions of LGM) but show little agreement regarding the ice-sheet sensitivity and inter-annual variability.

The CW pseudo accumulation record is further compared with accumulation at NGRIP accumulation rates (Fig. 11a), which have been calculated using layer thicknesses based on the Greenland Ice Core Chronology 2005 (GICC05) age scale (Andersen et al., 2006), which have been transformed to accumulation rates using a simple Dansgaard–Johnsen model with the ice thickness $H = 3085$ m ice equivalent (NGRIP members, 2004) and the model parameter $h = 500$ m ice equivalent. A density of $0.85\,\mathrm{kg\,L^{-1}}$ was used for the depth where preindustrial ice is found and $0.917\,\mathrm{kg\,L^{-1}}$ for the early Holocene and the LGM to convert to accumulation rates in m water equivalent.

With respect to PD, the mean accumulation in all three regions in the PI simulation is reduced by about 20–30 %, which is explained by a cooler and drier climate all over the NH polar regions simulated for PI conditions. The PI-PD mean accumulation difference has to be regarded as thermodynamically driven as we see no major change in the mean circulation. We expect that the mean accumulation difference is larger in the simulations representing equilibrium states than in observations due to the fact that part of the response to the PI-PD GHG forcing in the real world is still not fully active. However, the NGRIP as well as the NASA-U accumulation record (Anklin et al., 1998), which originate in the CW area (see Fig. 2), exhibit an increase in accumulation from pre-industrial to the present period. This is in agreement with the simulated CW accumulation response to global warming.

Comparing the PI with the $\mathrm{EH_{PD}}$ pseudo accumulation records, the early Holocene orbital forcing is observed to lead to a small increase in all three region's mean accumulation. Here, the accumulation growth is induced by the insolation-forced warmer

CPD
9, 3825–3870, 2013

summer temperatures during the early Holocene leading to an enhanced hydrological cycle and an increase in snowfall (see Fig. 4a) and consequently more accumulation, particularly in the CW and SE region. The different ice-sheet topographies in the EH sensitivity simulations also exhibit a distinct influence on the mean accumulation in all three records. This reveals that the amount of accumulation is very sensitive to changes in the local orography and that already comparatively small changes in GrIS topography are clearly reflected in the accumulation signal. Since changes in topography have a very local signature, they are one reason why accumulation records from different Greenland regions are not expected to conform on centennial to millennial time-scales. For example CW accumulation occurring with 7 ka topography is about 15 % higher than the equivalent with present topography (compare $EH_{7\,ka}$ and EH_{PD} in Fig. 11a) whereas in the SW region (Fig. 11b) accumulation in $EH_{7\,ka}$ is reduced by about 50 % reduced with respect to EH_{PD}. CW accumulation simulated in $EH_{7\,ka}$, $EH_{8\,ka}$ and $EH_{9\,ka}$ does reasonably agree with NGRIP data for 7, 8 and 9 ka, respectively. The model results suggest that the observed increase in NGRIP accumulation from 9 to 7 ka might be caused by changes in the local topography.

As expected the largest difference in accumulation is recorded for changes between the interglacial and glacial climate states. In all three regions we observe an average drop from PI to LGM of about 80 %, which is in agreement with the NGRIP data. As already identified by Kapsner et al. (1995) the glacial-interglacial differences cannot solely be explained by thermodynamic effects. In the case of the LGM simulation, the presence of an extensive Laurentide ice sheet reveals a distinct reorganization of the atmospheric circulation. The resulting southward shift in the westerly storm tracks (Hofer et al., 2012a) leads to an amplification of the drying conditions over Greenland.

The Greenland pseudo accumulation records further reveal considerable magnitude of inter-annual variability. In agreement with Crüger et al. (2004) and Hutterli et al. (2005), this study confirms that the inter-annual accumulation variability can be attributed to dynamical features, i.e. variability in the atmospheric circulation. Following the idea of Hutterli et al. (2005) we test whether years with anomalously high accumu-

CPD
9, 3825–3870, 2013

lation (spikes above upper dashed lines in Fig. 11) are consistently accompanied by the same atmospheric pattern with respect to years with anomalous low accumulation (spikes below lower dashed lines in Fig. 11). However, the circulation patterns accounting for the annual accumulation variability are not stable in all simulated climate states due to sub-seasonal effects. One caveat, however, is the fact that the model shows limited ability in reproducing the circulation patterns found for the reanalysis (Fig. 7), in particular for the accumulation variability in the CW region. The expansion of the analysis to the seasonal-scale reveals that the model is actually able to reproduce the atmospheric patterns responsible for accumulation variability within the different seasons. Further the model agrees with ERAi regarding the daily circulation-accumulation relationship on the synoptic-scale. This increases our confidence that the model captures the dynamical situation leading to a precipitation event. The model's difficulties in the representation of the annual relationship are attributed to differences in the contribution of the different seasons to the annual variability signal (see Sect. 4.2 for more details).

Independent from these model limitations we have confidence in the following arguments concerning the conclusion that the approach by Hutterli et al. (2005) is not necessarily valid for different climate states: the relationship between local GrIS accumulation and large-scale circulation patterns exhibits a remarkable seasonal cycle in both ERAi and the model simulations. Within a season, the attributed circulation patterns show good agreement in all paleo simulations. However, since the seasonal signals can add-up differently to the annual signal (Fig. 9), we do not find a stable relationship between annual accumulation and annual circulation patterns except for the SE region. The contributions of the seasonal to the annual variability signal generally follows the accumulation mean: if a change in seasonality due to an alteration in the orbital parameters, e.g., during the early Holocene, results in more GrIS summer accumulation at the expense of winter accumulation, the seasonal accumulation variability signals change accordingly. Hence, the seasonal contributions to the annual accumulation variability in any Greenland region cannot be expected to be constant over longer

CPD
9, 3825–3870, 2013

time periods. This implies that the composites in the annual accumulation records (as indicated in the different time-slices in Fig. 11) have to be treated very carefully regarding their interpretation since they likely differ due to sub-seasonal effects. The observed seasonality further indicates that using a proxy to describe the annual mean state of the atmospheric circulation is not very meaningful.

6 Conclusions

In the course of this paper, the sensitivity of GrIS accumulation to various forcings, e.g., changes in orbital forcing or the ice sheet topography is presented by climate simulations for the present, pre-industrial, the early Holocene, and the LGM. A second focus is set on the relationship of local accumulation variability and large-scale circulation patterns and its stability throughout the paleo simulations. The obtained key results have important implications for accumulation and other precipitation proxy records derived from Greenland ice cores: Greenland accumulation generally reacts very sensitively to all tested external forcing factors. Thereby, the accumulation changes due to any forcing exhibits strong spatial variability showing that accumulation records from different ice core sites cannot be expected to be coherent since they include an important local characteristic.

Both, changes in the mean and year-to-year variability of accumulation are dominated by snowfall whereas the impact of sublimation is an order of magnitude smaller. Changes in mean accumulation between different climate periods are driven by both thermodynamic and dynamic factors. Regarding the thermodynamic impact, a warming is generally accompanied by an increase in precipitation. As long as this precipitation falls in form of snow, the warming results in an accumulation increase as the increase in sublimation due to the warming cannot compensate for the additional snow mass. Dynamic drivers of accumulation changes are either changes in the large-scale circulation or in the local orography having a distinct imprint on the amount of precipitation deposited in any GrIS region. The variety of processes affecting precipitation and ac-

CPD
9, 3825–3870, 2013

cumulation on Greenland is certainly a challenge for the interpretation of long-term records.

Inter-annual accumulation and precipitation variability is consistently explained by the variability in the atmospheric circulation. Following the idea by Hutterli et al. (2005) we find distinct large-scale circulation patterns for three Greenland regions accounting for local accumulation variability. However, the relationship exhibits a distinct seasonal cycle showing that winter accumulation is accompanied by different patterns than summer accumulation. Further the contributions of the different seasons to annual variability signal varies during different climate states. As a consequence, the annual relationship used in previous studies (e.g., Appenzeller et al., 1998b; Hutterli et al., 2005) suffers from this seasonality and should not be applied on longer accumulation records from Greenland ice cores. However, we find significant stability in the seasonal relationship between large-scale circulation variability and their imprint in local GrIS accumulation or precipitation.

It is also shown that on the daily-scale a precipitation event in any of the tested Greenland regions is in all climate states associated with the same weather situation. Hence, we indeed see potential to reconstruct seasonal circulation patterns from ice core data. This approach, however, requires a precipitation proxy which resolves single seasons and which is explicitly dominated by wet deposition. To our knowledge, such a proxy a record has not been established yet. However, new high-resolution records of various chemical species from the NEEM ice core might offer the opportunity to reconstruct the occurrence of distinct seasonal large-scale circulation patterns as proposed in this work.

Acknowledgements. We acknowledge the Swiss National Supercomputing Centre (CSCS) for providing the supercomputing facilities. The ERA-Interim and ERA-40 re-analysis data were obtained from the European Centre for Medium-Range Weather Forecasts (ECMWF) data archive. This work is supported by funding to the Past4Future project from the European Commission's 7th Framework Programme. Grant number 243908 (2010–2014).

CPD
9, 3825–3870, 2013

References

Andersen, K. K., Svensson, A., Johnsen, S. J., Rasmussen, S. O., Bigler, M., Rothlisberger, R., Ruth, U., Siggaard-Andersen, M. L., Steffensen, J. P., Dahl-Jensen, D., Vinther, B. M., and Clausen, H. B.: The Greenland ice core chronology 2005, 15–42 ka. Part 1: Constructing the time scale, Quaternary Sci. Rev., 25, 3246–3257, doi:10.1016/j.quascirev.2006.08.002, 2006. 3847

Anklin, M., Bales, R. C., Mosley-Thompson, E., and Steffen, K.: Annual accumulation at two sites in northwest Greenland during recent centuries, J. Geophys. Res.-Atmos., 103, 28775–28783, doi:10.1029/98JD02718, 1998. 3827, 3847

Appenzeller, C., Schwander, J., Sommer, S., and Stocker, T. F.: The North Atlantic Oscillation and its imprint on precipitation and ice accumulation in Greenland, Geophys. Res. Lett., 25, 1939–1942, doi:10.1029/98GL01227, 1998a. 3827

Appenzeller, C., Stocker, T. F., and Anklin, M.: North Atlantic oscillation dynamics recorded in Greenland ice cores, Science, 282, 446–449, doi:10.1126/science.282.5388.446, 1998b. 3827, 3851

Bales, R. C., Guo, Q. H., Shen, D. Y., McConnell, J. R., Du, G. M., Burkhart, J. F., Spikes, V. B., Hanna, E., and Cappelen, J.: Annual accumulation for Greenland updated using ice core data developed during 2000–2006 and analysis of daily coastal meteorological data, J. Geophys. Res.-Atmos., 114, D06116, doi:10.1029/2008JD011208, 2009. 3834

Banta, J. R. and McConnell, J. R.: Annual accumulation over recent centuries at four sites in central Greenland, J. Geophys. Res.-Atmos., 112, D10114, doi:10.1029/2006JD007887, 2007. 3827

Berger, A. L.: Long-term Variations of Daily Insolation and Quaternary Climatic Changes, J. Atmos. Sci., 35, 2362–2367, doi:10.1175/1520-0469(1978)035<2362:LTVODI>2.0.CO;2, 1978. 3831, 3857

Braconnot, P., Otto-Bliesner, B., Harrison, S., Joussaume, S., Peterchmitt, J.-Y., Abe-Ouchi, A., Crucifix, M., Driesschaert, E., Fichefet, Th., Hewitt, C. D., Kageyama, M., Kitoh, A., Laîné, A., Loutre, M.-F., Marti, O., Merkel, U., Ramstein, G., Valdes, P., Weber, S. L., Yu, Y., and Zhao, Y.: Results of PMIP2 coupled simulations of the Mid-Holocene and Last Glacial Maximum – Part 1: experiments and large-scale features, Clim. Past, 3, 261–277, doi:10.5194/cp-3-261-2007, 2007. 3830, 3831, 3835

CPD
9, 3825–3870, 2013

Chen, L. L., Johannessen, O. M., Wang, H. J., and Ohmura, A.: Accumulation over the Greenland Ice Sheet as represented in reanalysis data, Adv. Atmos. Sci., 28, 1030–1038, doi:10.1007/s00376-010-0150-9, 2011. 3834

Crüger, T., Fischer, H., and von Storch, H.: What do accumulation records of single ice cores in Greenland represent?, J. Geophys. Res.-Atmos., 109, D21110, doi:10.1029/2004JD005014, 2004. 3827, 3848

Dee, D. P., Uppala, S. M., Simmons, A. J., Berrisford, P., Poli, P., Kobayashi, S., Andrae, U., Balmaseda, M. A., Balsamo, G., Bauer, P., Bechtold, P., Beljaars, A. C. M., van de Berg, L., Bidlot, J., Bormann, N., Delsol, C., Dragani, R., Fuentes, M., Geer, A. J., Haimberger, L., Healy, S. B., Hersbach, H., Hólm, E. V., Isaksen, L., Kållberg, P., Köhler, M., Matricardi, M., McNally, A. P., Monge-Sanz, B. M., Morcrette, J.-J., Park, B.-K., Peubey, C., de Rosnay, P., Tavolato, C., Thépaut, J.-N., and Vitart, F.: The ERA-Interim reanalysis: configuration and performance of the data assimilation system, Q. J. Roy. Meteor. Soc., 137, 553–597, doi:10.1002/qj.828, 2011. 3829

Dethloff, K., Schwager, M., Christensen, J. H., Kilsholm, S., Rinke, A., Dorn, W., Jung-Rothenhausler, F., Fischer, H., Kipfstuhl, S., and Miller, H.: Recent Greenland accumulation estimated from regional climate model simulations and ice core analysis, J. Climate, 15, 2821–2832, 2002. 3834

Fischer, N. and Jungclaus, J. H.: Evolution of the seasonal temperature cycle in a transient Holocene simulation: orbital forcing and sea-ice, Clim. Past, 7, 1139–1148, doi:10.5194/cp-7-1139-2011, 2011. 3835

Gent, P. R., Danabasoglu, G., Donner, L. J., Holland, M. M., Hunke, E. C., Jayne, S. R., Lawrence, D. M., Neale, R. B., Rasch, P. J., Vertenstein, M., Worley, P. H., Yang, Z. L., and Zhang, M. H.: The community climate system model version 4, J. Climate, 24, 4973–4991, doi:10.1175/2011JCLI4083.1, 2011. 3829

Hakuba, M. Z., Folini, D., Wild, M., and Schar, C.: Impact of Greenland's topographic height on precipitation and snow accumulation in idealized simulations, J. Geophys. Res.-Atmos., 117, D09107, doi:10.1029/2011JD017052, 2012. 3834

Hofer, D., Raible, C. C., Dehnert, A., and Kuhlemann, J.: The impact of different glacial boundary conditions on atmospheric dynamics and precipitation in the North Atlantic region, Clim. Past, 8, 935–949, doi:10.5194/cp-8-935-2012, 2012a. 3830, 3836, 3848

CPD
9, 3825–3870, 2013

Hofer, D., Raible, C. C., Merz, N., Dehnert, A., and Kuhlemann, J.: Simulated winter circulation types in the North Atlantic and European region for preindustrial and glacial conditions, Geophys. Res. Lett., 39, L15805, doi:10.1029/2012GL052296, 2012b. 3830, 3836, 3844

Hunke, E. C. and Lipscomb, W. H.: CICE: The Los Alamos Sea Ice Model, Documentation and Software User's Manual, Version 4.0, Los Alamos National Laboratory, Tech. Rep. LA-CC-06-012., 76 pp., 2008. 3830

Hutterli, M. A., Raible, C. C., and Stocker, T. F.: Reconstructing climate variability from Greenland ice sheet accumulation: an ERA40 study, Geophys. Res. Lett., 32, L23712, doi:10.1029/2005GL024745, 2005. 3828, 3833, 3838, 3846, 3848, 3849, 3851, 3861

Hutterli, M. A., Crueger, T., Fischer, H., Andersen, K. K., Raible, C. C., Stocker, T. F., Siggaard-Andersen, M. L., McConnell, J. R., Bales, R. C., and Burkhart, J. F.: The influence of regional circulation patterns on wet and dry mineral dust and sea salt deposition over Greenland, Clim. Dynam., 28, 635–647, 2007. 3827

Kapsner, W. R., Alley, R. B., Shuman, C. A., Anandakrishnan, S., and Grootes, P. M.: Dominant influence of atmospheric circulation on snow accumulation in Greenland over the past 18 000 years, Nature, 373, 52–54, doi:10.1038/373052a0, 1995. 3827, 3848

Lehner, F., Raible, C. C., and Stocker, T. F.: Testing the robustness of a precipitation proxy-based North Atlantic Oscillation reconstruction, Quaternary Sci. Rev., 45, 85–94, doi:10.1016/j.quascirev.2012.04.025, 2012. 3828

Luterbacher, J., Xoplaki, E., Dietrich, D., Jones, P. D., Davies, T. D., Portis, D., Gonzalez-Rouco, J. F., von Storch, H., Gyalistras, D., Casty, C., and Wanner, H.: Extending North Atlantic Oscillation reconstructions back to 1500, Atmos. Sci. Lett., 2, 114–124, doi:10.1006/asle.2001.0044, 2001. 3827

McConnell, J. R., Arthern, R. J., Mosley-Thompson, E., Davis, C. H., Bales, R. C., Thomas, R., Burkhart, J. F., and Kyne, J. D.: Changes in Greenland ice sheet elevation attributed primarily to snow accumulation variability, Nature, 406, 877–879, doi:10.1038/35022555, 2000a.

McConnell, J. R., Mosley-Thompson, E., Bromwich, D. H., Bales, R. C., and Kyne, J. D.: Interannual variations of snow accumulation on the Greenland Ice Sheet (1985–1996): new observations versus model predictions, J. Geophys. Res.-Atmos., 105, 4039–4046, doi:10.1029/1999JD901049, 2000b.

Merkel, U., Prange, M., and Schulz, M.: ENSO variability and teleconnections during glacial climates, Quaternary Sci. Rev., 29, 86–100, doi:10.1016/j.quascirev.2009.11.006, 2010. 3831

CPD
9, 3825–3870, 2013

Mosley-Thompson, E., McConnell, J. R., Bales, R. C., Lin, P. N., Steffen, K., Thompson, L. G., Edwards, R., and Bathke, D.: Local to regional-scale variability of annual net accumulation on the Greenland ice sheet from PARCA cores, J. Geophys. Res.-Atmos., 106, 33839–33851, doi:10.1029/2001JD900067, 2001. 3827

Neale, R. B., Richter, J. H., Conley, A. J., Park, S., Lauritzen, P. H., Gettelman, A., Rasch, P. J., Vavrus, J., S., Taylor, M. A., C., Zhang, M., and Lin, S.: Description of the NCAR Community Atmosphere Model (CAM4), National Center for Atmospheric Research, Tech. Rep. NCAR/TN+STR, 194 pp., 2010. 3829

NGRIP members: High-resolution record of Northern Hemisphere climate extending into the last interglacial period, Nature, 431, 147–151, doi:10.1038/nature02805, 2004. 3847, 3870

Oleson, K., Lawrence, D., Bonan, G., Flanner, M., Kluzek, E., Lawrence, P., Levis, S., Swenson, S., Thornton, P., Dai, A., Decker, M., Dickinson, R., Feddema, J., Heald, C., Hoffman, J.-F., Mahowald, N., Niu, G.-Y., Qian, T., Randerson, J., Running, S., Sakaguchi, K., Slater, A., Stockli, R., Wang, A., Yang, Z.-L., Zeng, X., and Zeng, X.: Technical Description of version 4.0 of the Community Land Model (CLM), National Center for Atmospheric Research, Technical Note NCAR/TN-478+STR, 257 pp., 2010. 3829

Peltier, W. R.: Global glacial isostasy and the surface of the ice-age earth: The ice-5G (VM2) model and grace, Annu. Rev. Earth Pl. Sc., 32, 111–149, doi:10.1146/annurev.earth.32.082503.144359, 2004. 3828, 3832, 3857, 3860

Pinto, J. G. and Raible, C. C.: Past and recent changes in the North Atlantic oscillation, Wiley Interdisciplinary Reviews – Climate Change, 3, 79–90, doi:10.1002/wcc.150, 2012. 3827

Raible, C. C., Casty, C., Luterbacher, J., Pauling, A., Esper, J., Frank, D. C., Buntgen, U., Roesch, A. C., Tschuck, P., Wild, M., Vidale, P. L., Schar, C., and Wanner, H.: Climate variability-observations, reconstructions, and model simulations for the Atlantic-European and Alpine region from 1500–2100AD, Climatic Change, 79, 9–29, doi:10.1007/s10584-006-9061-2, 2006. 3827

Rogers, J. C., Bathke, D. J., Mosley-Thompson, E., and Wang, S. H.: Atmospheric circulation and cyclone frequency variations linked to the primary modes of Greenland snow accumulation, Geophys. Res. Lett., 31, L23 208, doi:10.1029/2004GL021048, 2004. 3827

Smith, D., Harrison, S., Firth, C., and Jordan, J.: The early Holocene sea level rise, Quaternary Sci. Rev., 30, 1846–1860, 2011. 3830

Uppala, S. M., Kallberg, P. W., Simmons, A. J., Andrae, U., Bechtold, V. D., Fiorino, M., Gibson, J. K., Haseler, J., Hernandez, A., Kelly, G. A., Li, X., Onogi, K., Saarinen, S., Sokka, N.,

CPD
9, 3825–3870, 2013

Allan, R. P., Andersson, E., Arpe, K., Balmaseda, M. A., Beljaars, A. C. M., Van De Berg, L., Bidlot, J., Bormann, N., Caires, S., Chevallier, F., Dethof, A., Dragosavac, M., Fisher, M., Fuentes, M., Hagemann, S., Holm, E., Hoskins, B. J., Isaksen, L., Janssen, P. A. E. M., Jenne, R., McNally, A. P., Mahfouf, J. F., Morcrette, J. J., Rayner, N. A., Saunders, R. W., Simon, P., Sterl, A., Trenberth, K. E., Untch, A., Vasiljevic, D., Viterbo, P., and Woollen, J.: The ERA-40 re-analysis, Q. J. Roy. Meteor. Soc., 131, 2961–3012, doi:10.1256/qj.04.176, 2005. 3829

Varma, V., Prange, M., Merkel, U., Kleinen, T., Lohmann, G., Pfeiffer, M., Renssen, H., Wagner, A., Wagner, S., and Schulz, M.: Holocene evolution of the Southern Hemisphere westerly winds in transient simulations with global climate models, Clim. Past, 8, 391–402, doi:10.5194/cp-8-391-2012, 2012. 3831, 3832

Yeager, S. G., Shields, C. A., Large, W. G., and Hack, J. J.: The low-resolution CCSM3, J. Climate, 19, 2545–2566, doi:10.1175/JCLI3744.1, 2006. 3831

Yiou, P., Servonnat, J., Yoshimori, M., Swingedouw, D., Khodri, M., and Abe-Ouchi, A.: Stability of weather regimes during the last millennium from climate simulations, Geophys. Res. Lett., 39, L08703, doi:10.1029/2012GL051310, 2012. 3843

CPD
9, 3825–3870, 2013

Table 1. List of model simulations and the forcing used in the experiments. Present-day levels are denoted as pd, pre-industrial levels as pi, respectively. The orbital parameters are calculated according to Berger (1978). SST and sea ice fields are outputs of corresponding fully-coupled CCSM3 simulations (see Sect. 2.4 for details). The LGM levels of the GHGs are following the PMIP protocol. Solar forcing is expressed as total solar irradiance (TSI) and all the values correspond to CCSM4 standard levels. The pd ice sheets are CCSM4 standard whereas all paleo ice sheets correspond to ICE-5G masks by Peltier (2004) as illustrated in Fig. 1.

Simulation	Orbital parameters	SST/sea ice	CO_2 [ppm]	CH_4 [ppb]	N_2O [ppb]	TSI [$W m^{-2}$]	Ice sheets
PD	pd	pd	354	1694	310	1361.8	pd
PI	pd	pi	280	760	270	1360.9	pd
EH_{PD}	8 ka	8 ka	280	760	270	1360.9	pd
$EH_{7\,ka}$	8 ka	8 ka	280	760	270	1360.9	7 ka
$EH_{8\,ka}$	8 ka	8 ka	280	760	270	1360.9	8 ka
$EH_{9\,ka}$	8 ka	8 ka	280	760	270	1360.9	9 ka
LGM	21 ka	21 ka	185	350	200	1360.9	21 ka

CPD
9, 3825–3870, 2013

Table 2. Annual means of hydrological parameters (in mm liquid water equivalent yr^{-1}) averaged over the Greenland ice sheet.

Simulation	Total precipitation	Snowfall	Sublimation	Accumulation
PD	471	400	54	346
PI	390	344	40	303
EH_{PD}	419	351	50	301
$EH_{7\,ka}$	419	350	57	293
$EH_{8\,ka}$	383	316	56	260
$EH_{9\,ka}$	373	327	47	280
LGM	113	105	17	88

CPD
9, 3825–3870, 2013

Table 3. Pattern correlation values of z500 composites for each model simulation vs. the present day (PD) simulation. The composite patterns are derived from the accumulation (annual and seasonal mean) and precipitation (daily) time series, respectively, for the CW, SW and SE region. The PD composite patterns used as reference to compare with are the ones shown in Fig. 10b, d (for daily precipitation variability in winter (DJF) and summer (JJA)), Fig. 8b, d (for winter and summer mean accumulation variability) and Fig. 7d, e, f (for annual mean accumulation variability). The domain used for the pattern correlation covers the North Atlantic area and Europe (see frame in Fig. 7). Note that italic values are significant at the 5 %-level using a conservative estimate derived from *t* test statistics and auto-correlation applied on the NA domain composites.

Simulation	DJF daily precipitation			JJA daily precipitation			DJF mean accumulation			JJA mean accumulation			annual mean accumulation		
	CW	SW	SE	CW	SW	SE	CW	SW	SE	CW	SW	SE	CW	SW	SE
PI	*0.96*	*0.96*	*0.96*	*0.92*	*0.97*	*0.95*	*0.86*	*0.52*	*0.57*	*0.55*	*0.76*	*0.85*	0.24	*0.40*	*0.77*
EH_{PD}	*0.97*	*0.98*	*0.97*	*0.95*	*0.95*	*0.95*	*0.87*	*0.75*	*0.59*	*0.76*	*0.68*	*0.78*	0.15	0.45	*0.59*
$EH_{7\,ka}$	*0.96*	*0.92*	*0.96*	*0.95*	*0.95*	*0.97*	*0.84*	*0.71*	*0.77*	*0.52*	*0.58*	*0.87*	0.03	*0.65*	*0.49*
$EH_{8\,ka}$	*0.90*	*0.90*	*0.94*	*0.95*	*0.97*	*0.95*	0.18	0.27	0.47	*0.65*	−0.10	*0.61*	0.29	*0.57*	*0.77*
$EH_{9\,ka}$	*0.97*	*0.97*	*0.95*	*0.96*	*0.97*	*0.96*	*0.66*	*0.79*	*0.78*	*0.65*	*0.61*	*0.50*	0.04	0.31	*0.84*
LGM	*0.72*	*0.94*	*0.80*	*0.78*	*0.82*	*0.65*	*0.71*	*0.78*	0.20	*0.53*	*0.58*	0.26	0.09	0.40	*0.69*

CPD
9, 3825–3870, 2013

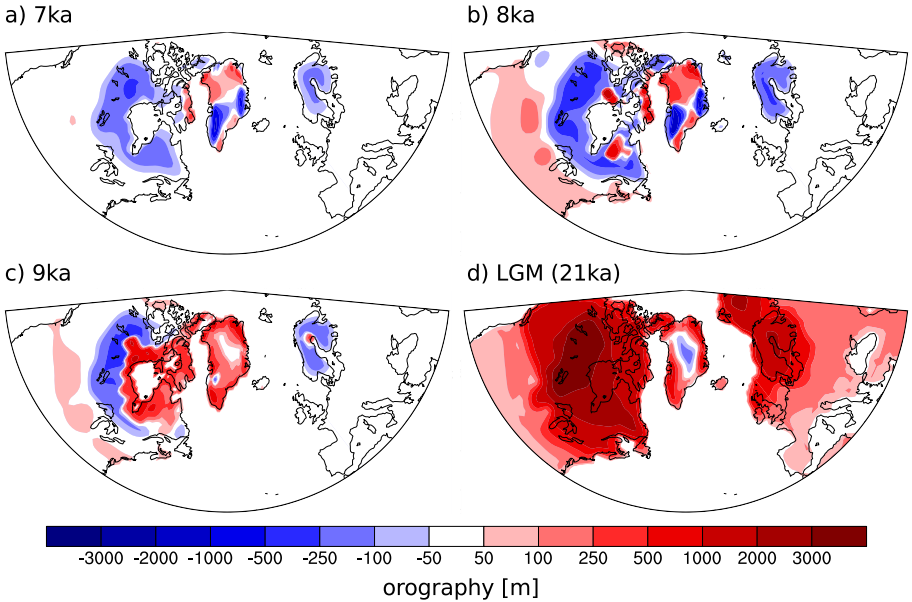

Fig. 1. Paleo topographies implemented in the model simulations: Deviation from present-day mask [m] for **(a)** 7 ka, **(b)** 8 ka, **(c)** 9 ka and **(d)** LGM (21 ka). All topographies are based on output from the ICE-5G model by Peltier (2004).

CPD
9, 3825–3870, 2013

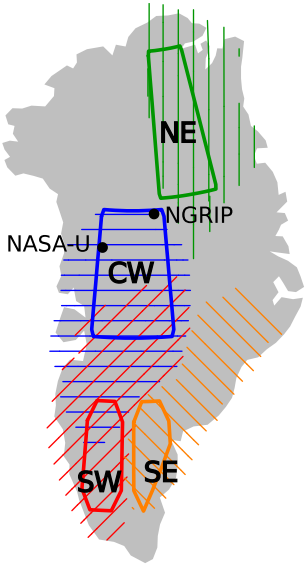

Fig. 2. Overview of the Greenland accumulation regions (frames) as defined in Hutterli et al. (2005). For each region accumulation is averaged over the included grid cells to come up with a single pseudo accumulation record. The shaded areas denote regions which show a coherent accumulation behavior as the pseudo record of the corresponding region (correlation of ≥ 0.7 in ERAi). The two dots indicate the locations of the NASA-U and the NGRIP ice cores.

CPD
9, 3825–3870, 2013

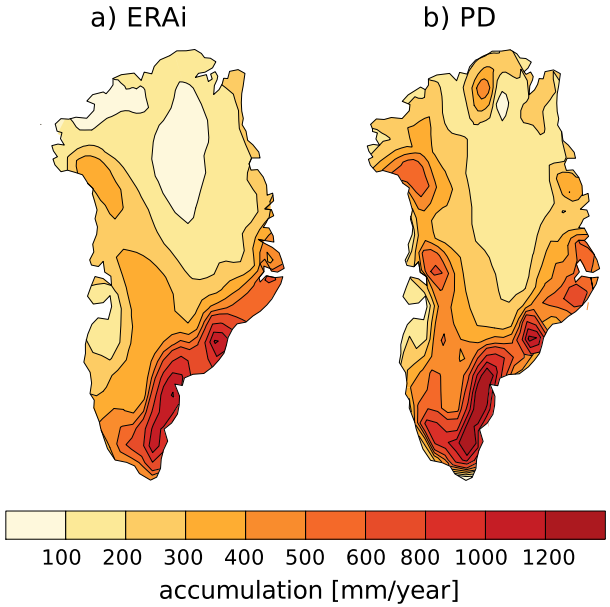

Fig. 3. Annual mean accumulation [mm yr^{-1}] over the Greenland ice sheet for **(a)** ERAi and **(b)** PD simulation.

CPD
9, 3825–3870, 2013

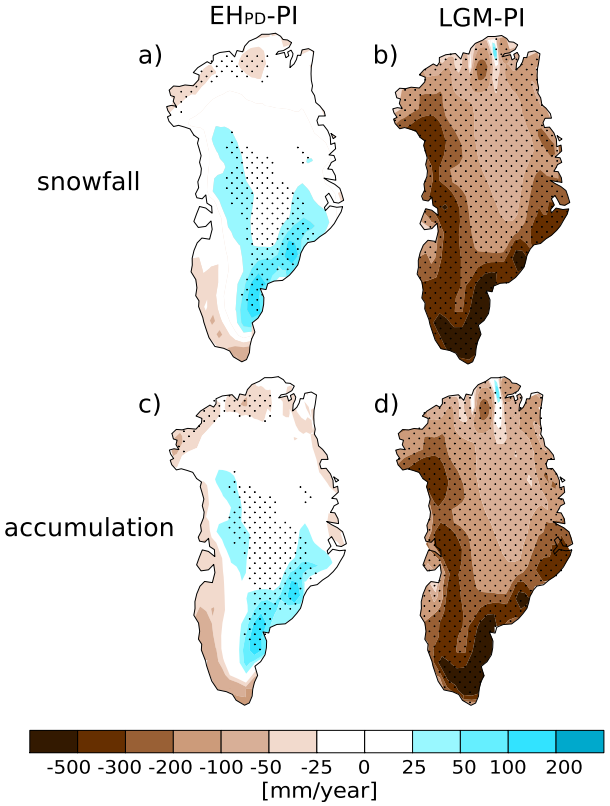

Fig. 4. Annual mean **(a, b)** snowfall and **(c, d)** accumulation [mm yr^{-1}] for EH_{PD}-PI and LGM-PI. Stippling denotes values significant at the 5 % level based on *t* test statistics.

CPD
9, 3825–3870, 2013

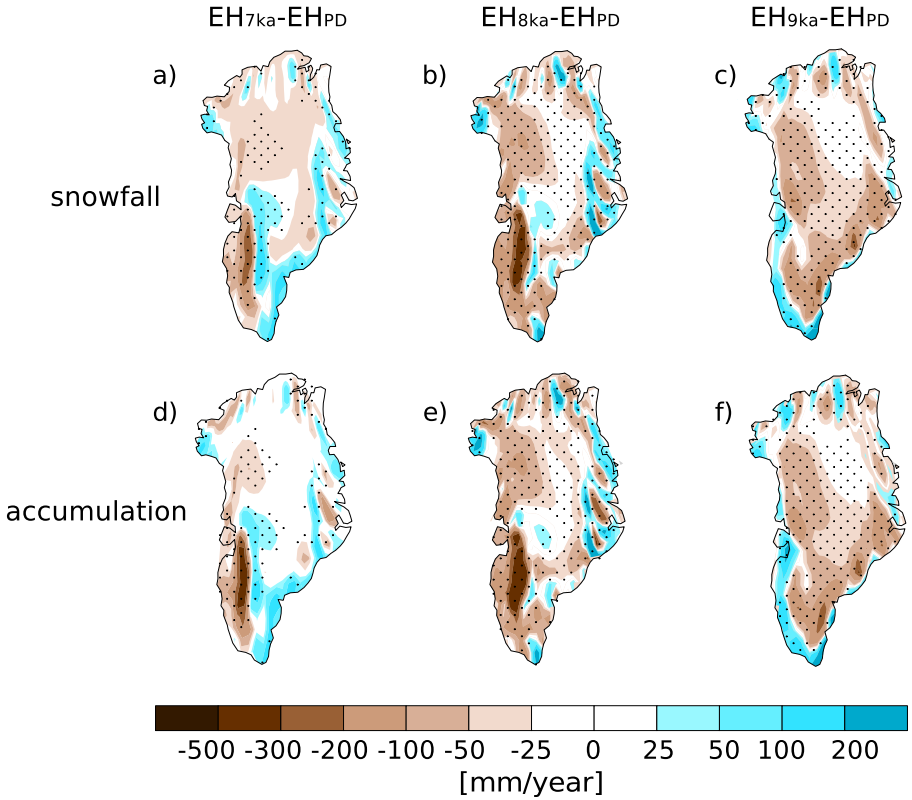

Fig. 5. Early Holocene ice sheet sensitivity of annual mean **(a, b, c)** snowfall and **(d, e, f)** accumulation [mm yr^{-1}] for the simulations with 7, 8 and 9 ka ice sheet topography. All values are anomalies from the basic early Holocene simulation (EH_{PD}) with present-day Greenland ice sheet. Stippling denotes values significant at the 5 % level based on *t* test statistics.

CPD
9, 3825–3870, 2013

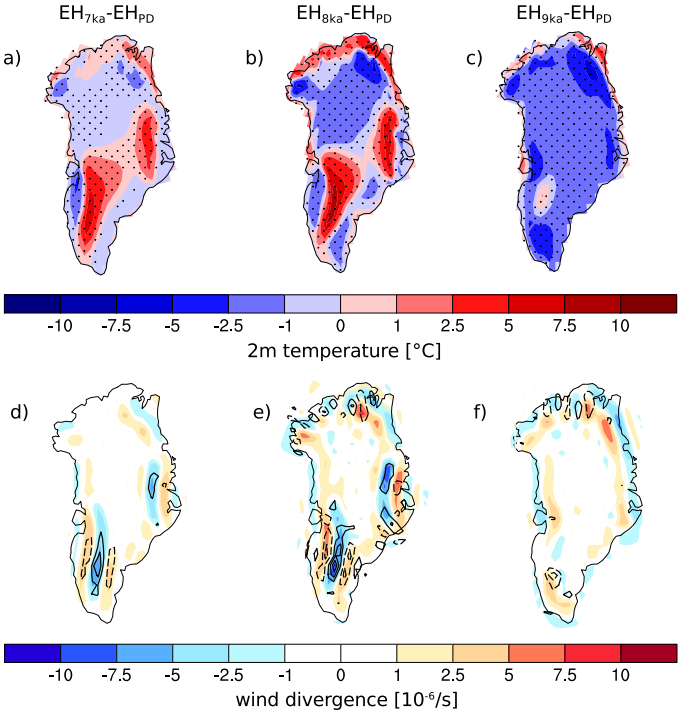

Fig. 6. Early Holocene ice sheet sensitivity of annual mean **(a, b, c)** 2 m temperature [°C] and **(d, e, f)** wind divergence [10^{-6} s^{-1}] over the Greenland ice sheet for the simulations with 7, 8 and 9 ka ice sheet topography. All values are anomalies from the basic early Holocene simulation (EH_{PD}) with present-day Greenland ice sheet. Stippling in **(a, b, c)** denotes values significant at the 5 % level based on *t* test statistics. In **(d, e, f)** the shading denotes wind divergence at 850 hPa and contour lines represent wind divergence at 500 hPa with negative contours stippled and no zero line shown. Areas with negative (positive) wind divergence at the surface (at higher levels) experience local upward flow. Vice-versa, areas with positive (negative) wind divergence at the surface (at higher levels) experience local downward flow.

CPD
9, 3825–3870, 2013

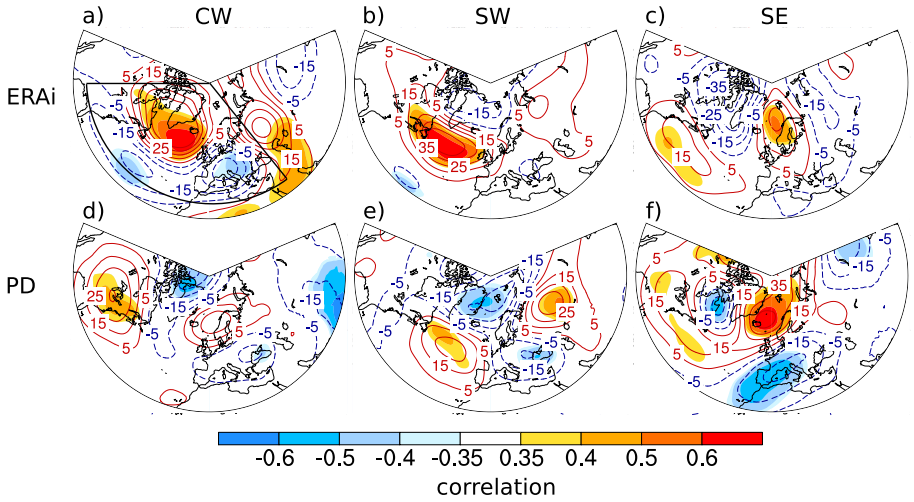

Fig. 7. z500 correlation and plus-minus composite patterns associated with annual mean accumulation in CW, SW and SE for **(a, b, c)** ERAi and **(d, e, f)** the PD simulation. The shading illustrates the correlation pattern significant at the 5 % level (t test statistics). Contour lines illustrate the z500 plus-minus composite pattern (in geopotential height meters). The plus-minus composite corresponds to the difference pattern of the ±1 standard deviation samples of annual mean accumulation. The framed area in CW **(a)** indicates the North Atlantic domain used by the pattern correlation analysis.

CPD
9, 3825–3870, 2013

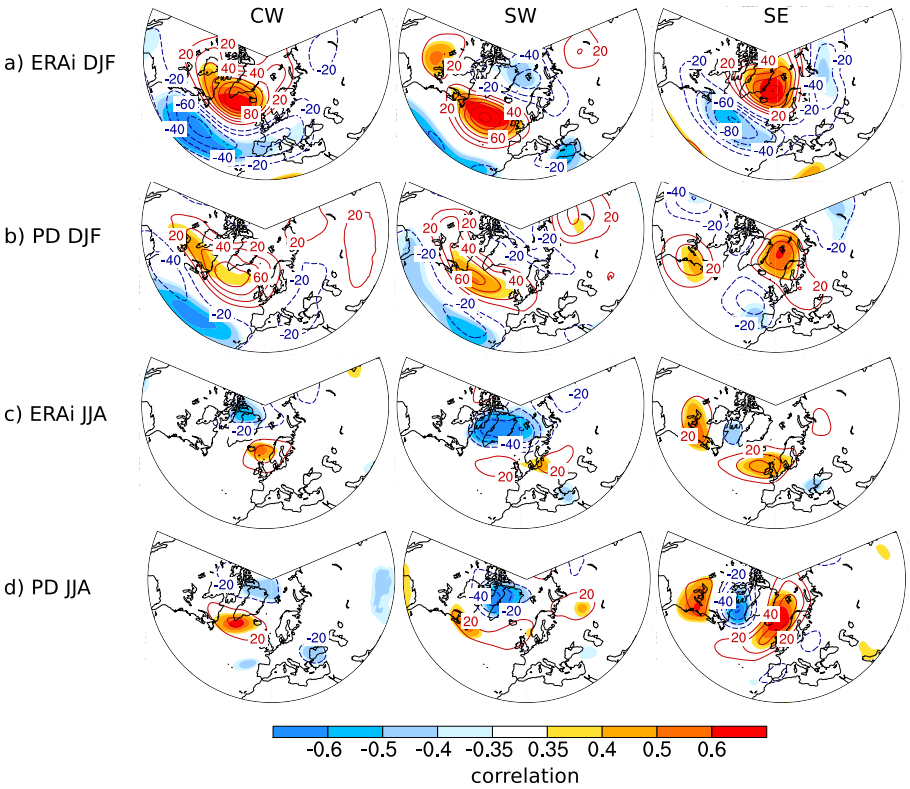

Fig. 8. z500 correlation and plus-minus composite patterns associated with seasonal mean accumulation in CW, SW and SE for **(a)** ERAi winters (DJF), **(b)** PD winters, **(c)** ERAi summers (JJA) and **(d)** PD summers. As in Fig. 7 shading illustrates the correlation pattern significant at the 5 % level (*t* test statistics) and contour lines illustrate the z500 plus-minus composite (in geopotential height meters). The plus-minus composite corresponds to the difference pattern of the ±1 standard deviation samples of seasonal mean accumulation.

CPD
9, 3825–3870, 2013

Fig. 9. Seasonal contribution to annual accumulation variability of the pseudo accumulation records in the **(a)** central-western (CW), **(b)** south-western (SW) and **(c)** south-eastern (SE) region for ERAi and all simulations. Note that these seasonal contributions are calculated as standard deviations of the according seasonal mean accumulation time series. They are all expressed as relative portions of 100 %.

CPD
9, 3825–3870, 2013

Greenland accumulation links to atmospheric circulation

N. Merz et al.

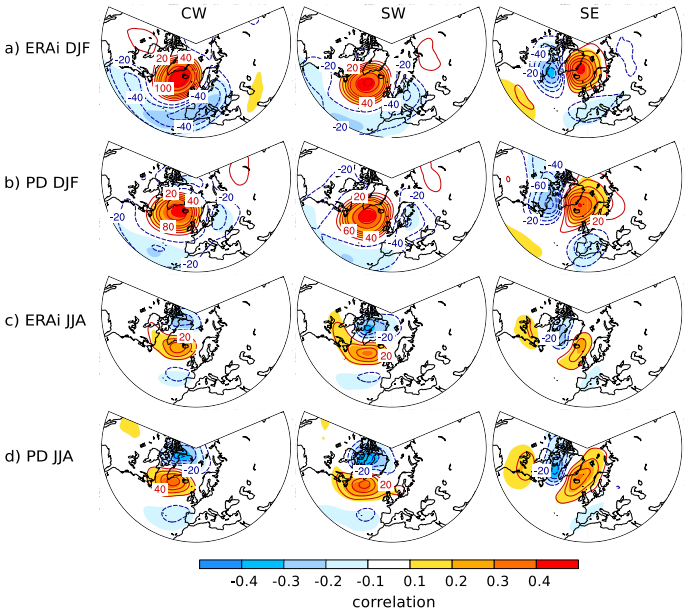

Fig. 10. z500 correlation and positive composite patterns associated with daily precipitation in CW, SW and SE for **(a)** ERAi winters (DJF), **(b)** PD winters, **(c)** ERAi summers (JJA) and **(d)** PD summers. The shading illustrates the correlation pattern for values ≥ 0.1, respectively ≤ -0.1 (significant at the 1 % level due to the large sample size of ≥ 2700 days for each season). Contour lines illustrate the z500 positive composite (in geopotential height meters) expressed as anomaly from the seasonal climatology. The positive composite samples all days with ≥ 1 standard deviation in daily precipitation.

CPD
9, 3825–3870, 2013

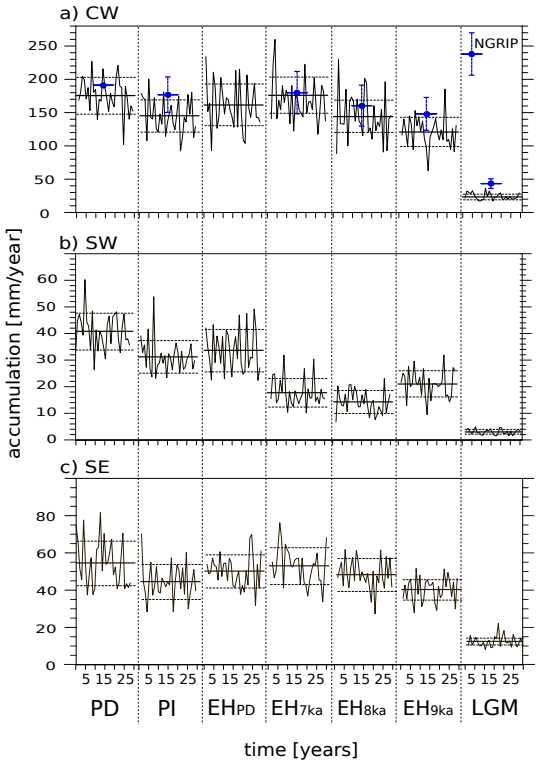

Fig. 11. Pseudo accumulation records for the **(a)** CW, **(b)** SW and **(c)** SE Greenland region with annual mean accumulation [mm day^{-1}] in the different model simulations. The solid reference lines denote the 30 yr time-slice mean accumulation whereas the stippled lines denote ±1 standard deviation values. Note that due to the time-slice setup, the records are not continuous. In **(a)** the blue dots with error bars indicate the NGRIP accumulation rates determined for, present, pre-industrial, 7, 8, 9 and 21 ka. The present NGRIP accumulation rate of 0.19 m has been determined by NGRIP members (2004).

CPD
9, 3825–3870, 2013